Spectroscopic spectral-domain optical coherence microscopy

Chengyang Xu, Claudio Vinegoni, Tyler S. Ralston, Wei Luo, Wei Tan, and Stephen A. Boppart

Biophotonics Imaging Laboratory, Beckman Institute for Advanced Science and Technology, University of Illinois at Urbana-Champaign, 405 North Mathews Avenue, Urbana, Illinois 61801

Received October 13, 2005; revised December 30, 2005; accepted January 3, 2006; posted January 17, 2005 (Doc. ID 65352)

The spectroscopic content within optical coherence tomography (OCT) data can provide a wealth of information. Spectroscopic OCT methods are frequently limited by time-frequency trade-offs that limit high spectral and spatial resolution simultaneously. We present spectroscopic spectral-domain optical coherence microscopy performed with a multimodality microscope. Restricting the spatial extent of the signal by using high-numerical-aperture optics makes high-resolution spectroscopic information accessible, facilitated with spectral-domain detection. Simultaneous acquisition of multiphoton microscopy images is used to validate tissue structure and localization of nuclei within individual cells. © 2006 Optical Society of America

OCIS codes: 170.0180, 170.4500, 300.0300, 190.4180.

Spectroscopic optical coherence tomography (SOCT), a recent extension of OCT imaging, analyzes not only the intensities, but also the spectra of backscattered light in a depth-resolved manner.[1,2] This technique is capable of both qualitative contrast enhancement and quantitative concentration measurement.[3,4] Initial studies using SOCT were based on wavelength-dependent absorption by endogenous or exogenous absorbers that have well-defined absorption profiles. Recently, wavelength-dependent scattering has also been shown to be an important source of contrast that can be used not only for contrast enhancement, but also for particle sizing.[5,6] Compared with absorption-based SOCT imaging, scattering-based SOCT imaging has the advantage of enhanced stability, sensitivity, and localization.[6] However, there are two competing requirements for correctly interpreting scattering-based SOCT measurement in traditional SOCT systems. In order to utilize electromagnetic theories (e.g., Mie theory) in applications such as particle sizing, there must be a limited number of scatterers inside a SOCT analysis window. Because the density of scatterers in most tissue is typically very high, a small SOCT analysis window is therefore utilized. However, due to the trade-off of spectral resolution and spatial resolution in standard SOCT analysis, in order to identify dense spectral modulation for applications such as particle sizing, high spectral resolution is required, which implies the need for a large analysis window and subsequently a lower spatial resolution.

To solve this contradiction, algorithmic approaches have been implemented, but improvement is capped by a theoretical limit.[7,8] A feasible solution to this problem is to decouple the spectral resolution from the spatial resolution. A high-numerical-aperture (NA) lens is used to spatially limit light collection to within a small focal gate, while spectral-domain detection is used to collect spectral information in depth through the focus.[9] The heterodyne detection and coherence gating offered by optical coherence microscopy (OCM) increase the imaging penetration depth in scattering media by twofold or threefold over conventional confocal microscopy.[10] Spectroscopic analysis of spectral-domain OCM measurements, in combination with high-sensitivity intensity measurements afforded by traditional OCM, offers a potentially powerful tool for adding functional information to the structural information.[11]

A custom-designed and constructed multimodality microscope was used in this study, which enabled not only OCM and spectroscopic OCM (SOCM), but also simultaneous multiphoton microscopy using the same optical source.[12] The microscope objective ($20\times$, 0.95 NA, water immersion, Olympus) had a high NA in order to achieve high lateral resolution and tight spatial confinement of the backscattered OCM signal. Dispersion in the proprietary glass of the objective was balanced digitally. The interferometric setup was similar to those used in spectral-domain OCT.[9] In our configuration, a free-space 50/50 beam splitter was used. The optical spectrum was focused on a line-scan camera (L104k–2k, Basler, Inc.) that contained a 2048-element CCD array of detection elements with a maximum readout rate of 29 kHz. Digital processing of the detected signal included a spline interpolation to make the signal more uniform, and a discrete Fourier transform on each set of 2048, 10-bit values captured by the CCD to transform the signal from the frequency (spectral) domain into the spatial (depth) domain.

The axial point-spread function (PSF) of the objective using spectral-domain OCM detection was measured to be 2.2 μm at FWHM. Note that in our system the confocal gating (confocal parameter =2.2 μm) is below the coherence gating (coherence length =7 μm) with the laser source bandwidth of 40 nm. OCM images of a calibrated U.S. Air Force test target were used to determine the high transversal resolution (0.9 μm) by use of the edge-scan definition. The signal-to-noise ratio (SNR) was calculated by taking the ratio between the signal power and the noise variance. With 1 mW(0 dBm) of power incident on the mirror, the measured SNR was found to be equal to 97 dB. The dynamic range within experimental image data was approximately 60 dB. Calibrated fluorescent microbeads were used to determine the axial

0146-9592/06/081079-3/$15.00

and transverse multiphoton microscopy resolutions of our system, which were 0.8 and 0.5 μm, respectively. Incident optical power ranged from 1 to 5 mW (1 mW typical), with the higher power used to excite two-photon fluorescence from green-fluorescent protein (GFP).

The spectral-domain OCM interference fringes were acquired at 2048 pixels per OCM point, covering a potential full-array light spectral range from 740 to 860 nm, and which corresponded to an imaging depth of approximately 2.7 mm in air. The raw spectral-domain OCM interference is given by[13]

$$I(k,z)_{z=z_0} = 2[R_r R_s(k,z)_{z=z_0}]^{1/2} S(k)\cos(2k\Delta p),$$

where k is the free-space wavenumber, z is the depth, R_r and R_s are the reference reflectivity and sample reflectivity, respectively, $S(k)$ is the source spectral density, and Δp is the optical path-length difference at z_0 that is defined by the focal gating of the high-NA objective. The reference reflectivity R_r is assumed to be wavelength independent. The modulation transfer function of the spectral-domain OCM system was calibrated by using a mirror, and the raw spectral domain signal was remapped to k space by using cubic spline interpolation. The spectral-domain data were then demodulated to the base band by first taking the fast Fourier transform (FFT) to obtain the depth-dependent analytical signal, followed by the inverse FFT of the depth signal segment centered around the focal gate position. A Gaussian window of 512 points with a FWHM of 256 points was used, which corresponded to a spectral resolution of 0.5 nm.

The retrieved $R_s(k)$ at the focal plane of the OCM objective was processed by two different SOCM analysis methods. The first method was based on metameric imaging, where the scattering spectrum within the FWHM of the source spectrum was divided into three equally spaced subbands, and the intensity from the low-, mid-, and high-frequency bands were assigned to the red, green, and blue channels, respectively. We found this method represents information similar to the traditional spectral centroid method[2] but is more robust and more similar to the mechanism of human vision. The second method was based on spectral analysis initially proposed in light scattering spectroscopy (LSS).[14,15] The backscattered spectra were first analyzed by the FFT, and the first peak of the FFT data was used for hue information in a hue–saturation–value (HSV) color scale. This peak position is related to the physical size and interscatterer distance of the dominant scatterers, such as the nucleus, within the focal gate at that location. A comparison of SOCM signals (average of 100) detected from a fibroblast cell center (near the nucleus) and from the cell periphery (off the nucleus) is shown in Fig. 1. These two specific methods were chosen to represent two general types of possible spectroscopic spectral-domain OCM measurement. The metameric method is more qualitative and suited for attenuation-based measurements in SOCM, while the spectral analysis method used in LSS is more quantitative and suited for scattering-based measurements in SOCM.

These representative SOCM analysis methods were performed on spectral-domain OCM data collected from tissue and cell specimens imaged using our multimodality microscope. Figure 2 shows image data acquired from tissue from a rat, consisting of adjacent adipose (fat) and muscle tissue. The high-resolution OCM image shows individual adipocytes in the center of the image (Fig. 2A) but exhibits regions of low backscatter over more dense muscle tissue (Figs. 2A and 2B, upper right, lower left corners of images), possibly due to forward scattering or polarization-dependent effects. However, compared with OCM, the SOCM analysis methods (Figs. 2C and 2D) show increased contrast for muscle compared with the adipose tissue where there is sufficient backscattered signal for spectral analysis. This contrast enhancement (light yellow and blue regions in Fig. 2C, and green and blue regions in Fig. 2D) is due to different scatterer sizes and scatterer organization (likely nuclei and other organelles) and is more prominent in the SOCM image based on LSS spectral analysis (Fig. 2D, green regions), which has been shown to detect changes in nuclear regions.[14]

Spectroscopic OCM analysis methods are well suited for localizing dominant scatterers such as nuclei. We have investigated SOCM analysis at the single-cell level. Figure 3 shows an OCM image of live fibroblast cells in culture and the corresponding SOCM image from LSS spectral analysis (Figs. 3A and Fig. 3B), respectively). The first peak positions of the FFT obtained from the modulation patterns of the backscattered light are clearly different near the center of the cell, compared with the periphery of the cell. One possible reason for this difference is the presence of a large scatterer, the nucleus, located near the center of these cultured cells. We confirmed our SOCM findings by multiphoton imaging this cell culture, using the simultaneous multimodality capabilities of our microscope.[12] These transfected fibroblasts expressed GFP-labeled vinculin (a cell adhesion protein) and were colabeled with a DNA-specific dye (Hoechst 33342) for localization of nuclei relative to the surrounding cell structures (Fig. 3C). The si-

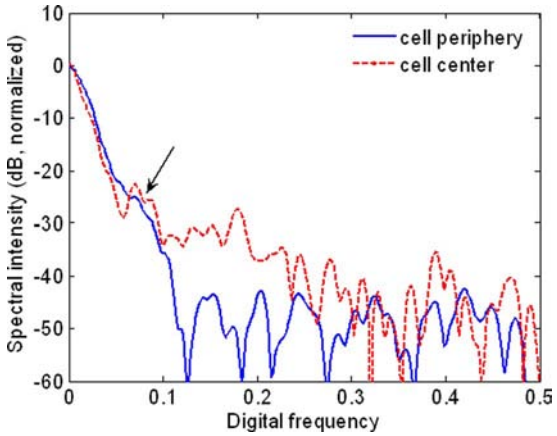

Fig. 1. (Color online) Spectral intensity curves. The arrow marks the first peak positions of the FFT of the backscattered light modulation patterns.

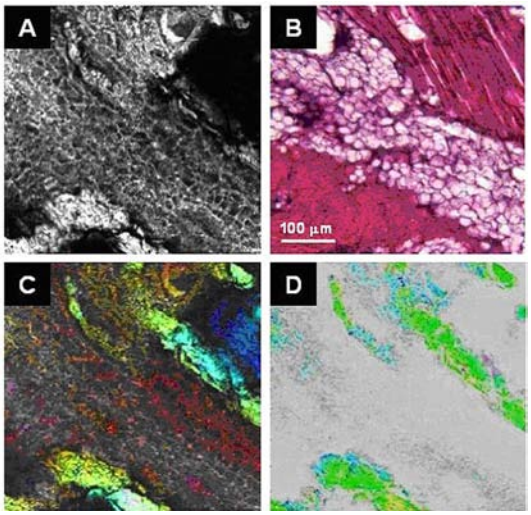

Fig. 2. (Color online) Spectroscopic spectral-domain OCM. A, OCM of rat tissue with regions of adipose cells (middle) and muscle (upper right, lower left). B, Corresponding histology. C, SOCM image using metameric spectral analysis. D, SOCM image using LSS spectral analysis. The scale bar is representative for all images.

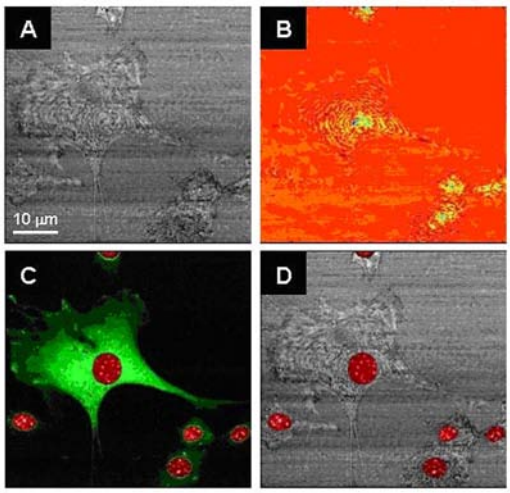

Fig. 3. (Color online) Single-cell imaging with spectroscopic spectral-domain OCM. A, Spectral-domain OCM of a GFP-vinculin transfected fibroblast. B, Corresponding SOCM image showing localized regions of strong spectral scattering. C, Multiphoton microscopy of GFP fibroblasts colabeled with DNA–nuclear dye. D, Overlay of multiphoton DNA-dye fluorescence and OCM images.

multaneous multimodality imaging afforded by our microscope can provide overlays of various image channels, as shown for OCM and the multiphoton fluorescence from the DNA–nuclear dye (Fig. 3D). The SOCM analysis information is consistent with the multiphoton imaging data in identifying the locations of the nuclei within these cells. Of the six nuclei identified in the multiphoton fluorescence image (Fig. 3C), five nuclei are clearly identified in the SOCM image (Fig. 3B, green–blue regions). The remaining cell nucleus (leftmost cell) may not be identified as clearly with SOCM, because this cell may be smaller and have a flatter profile than the others, resulting in a backscattering spectrum more similar to the background.

In conclusion, spectroscopic spectral-domain OCM analysis with tight focal gating decouples the inherent trade-off between spectral and spatial (depth) resolution. This allows the extraction of more minute spectroscopic features from within the small imaging volumes, making localized analysis of wavelength-dependent scattering possible. Wavelength-dependent scattering and the resulting spectral modulation are information-rich processes that are dependent on both optical properties of the scatterer and the interscatterer spacing. Our studies demonstrate that spectroscopic spectral-domain OCM is capable of enhancing contrast in various tissues and cells based solely on endogenous structures.

This work was supported in part by the National Institutes of Health (1 R01 EB00108, 1 R01 EB001777, S.A.B.) and the National Science Foundation (BES 03-47747, S.A.B.). C. Xu and C. Vinegoni contributed equally to this work.

References

1. R. Leitgeb, M. Wojtkowski, A. Kowalczyk, C. K. Hitzenberger, M. Sticker, and A. F. Fercher, Opt. Lett. **25**, 820 (2000).
2. U. Morgner, W. Drexler, F. C. Kartner, X. D. Li, C. Pitris, E. P. Ippen, and J. G. Fujimoto, Opt. Lett. **25**, 111 (2000).
3. C. Xu, J. Ye, D. L. Marks, and S. A. Boppart, Opt. Lett. **29**, 1647 (2004).
4. D. J. Faber, E. G. Mik, M. C. Aalders, and T. G. van Leeuwen, Opt. Lett. **30**, 1015 (2005).
5. D. C. Adler, T. H. Ko, P. R. Herz, and J. G. Fujimoto, Opt. Express **12**, 5487 (2004).
6. C. Xu, P. S. Carney, and S. A. Boppart, Opt. Express **13**, 5450 (2005).
7. C. Xu, F. Kamalabadi, and S. A. Boppart, Appl. Opt. **44**, 1813 (2005).
8. D. L. Jones and T. W. Parks, IEEE Trans. Signal Process. **40**, 413 (1992).
9. A. F. Fercher, C. K. Hitzenberger, G. Kamp, and S. Y. Elzaiat, Opt. Commun. **117**, 43 (1995).
10. J. A. Izatt, M. R. Hee, G. M. Owen, E. A. Swanson, and J. G. Fujimoto, Opt. Lett. **19**, 590 (1994).
11. R. A. Leitgeb, W. Drexler, B. Povazay, B. Hermann, H. Sattmann, and A. F. Fercher, in Proc. SPIE **5690**, 151 (2005).
12. C. Vinegoni, T. Ralston, W. Tan, W. Luo, D. L. Marks, and S. A. Boppart, Appl. Phys. Lett. **88**, 053901 (2006).
13. C. Joo, T. Akkin, B. Cense, B. H. Park, and J. F. de Boer, Opt. Lett. **30**, 2131 (2005).
14. A. Wax, C. Yang, and J. A. Izatt, Opt. Lett. **28**, 1230 (2003).
15. Y. Liu, X. Li, Y. L. Kim, and V. Backman, Opt. Lett. **30**, 2445 (2005).